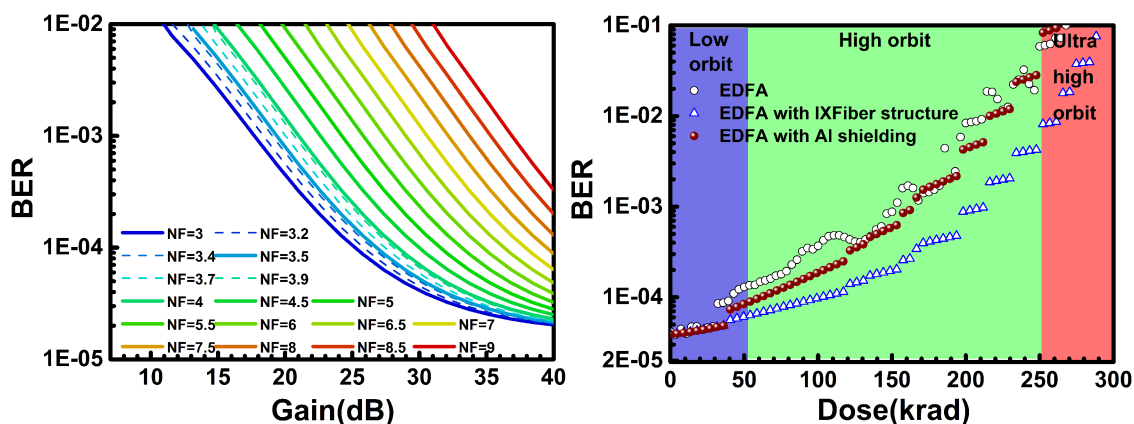


EDFA Anti-Irradiation Schemes for Inter-Satellite Optical DPSK Communication Systems


Volume 11, Number 3, June 2019

Baoluo Yan
Haifeng Liu
Bo Liu
Jianguo Liu
Hao Zhang
Chengkun Yang
Zonghua Hu
Xiaolong Li



DOI: 10.1109/JPHOT.2019.2916775
1943-0655 © 2019 IEEE

EDFA Anti-Irradiation Schemes for Inter-Satellite Optical DPSK Communication Systems

Baolu Yan ¹, Haifeng Liu ^{1,2}, Bo Liu ¹, Jianguo Liu ²,
Hao Zhang ¹, Chengkun Yang,¹ Zonghua Hu,¹ and Xiaolong Li¹

¹Tianjin Key Laboratory of Optoelectronic Sensor and Sensing Network Technology, Institute of Modern Optics, Nankai University, Tianjin 300350, China

²State Key Laboratory on Integrated Optoelectronics, Institute of Semiconductors, Chinese Academy of Sciences, Beijing 100083, China

DOI:10.1109/JPHOT.2019.2916775

1943-0655 © 2019 IEEE. Translations and content mining are permitted for academic research only.

Personal use is also permitted, but republication/redistribution requires IEEE permission.

See http://www.ieee.org/publications_standards/publications/rights/index.html for more information.

Manuscript received May 10, 2019; accepted May 11, 2019. Date of publication May 14, 2019; date of current version June 11, 2019. This work was supported in part by the National Natural Science Foundation of China under Grants 61727815, 11774181, and 61875091; in part by Science and Technology Support Project of Tianjin under Grant 16YFZCSF00400; and in part by the Opened Fund of the State Key Laboratory of Integrated Optoelectronics No. IOSKL2018KF18. Corresponding authors: Haifeng Liu and Bo Liu (e-mail: 016045@nankai.edu.cn; liubo@nankai.edu.cn).

Abstract: The uprising of rare-earth-doped fiber amplifier technology provides an effective solution to signal power compensation for interstellar optical communication systems, but significant signal power attenuation induced by spatial irradiation has ever been a significant issue to be resolved in practical applications. In order to explore the impact of radiation on the performances of high-speed differential phase shift keying (DPSK) satellite communication systems using EDFA preamplification technique, the irradiation effect on output central wavelength, half width, and noise figure (NF) of EDFA has been studied. Different anti-irradiation schemes employing Co^{60} radiation sources with a total radiation dose of up to 300 krad are compared from experimental perspective to optimize the anti-irradiation scheme. Radiation-induced attenuation (RIA) as well as increase in NF of the EDFA is considered in our simulation model, by which the limitations of the physical shielding scheme could be clarified and quantitatively evaluated. We conclude that compared to the RIA effect, the increase in noise figure plays a major role in the degradation of communication systems. In addition, according to simulation results of two high-speed DPSK systems, some anti-irradiation schemes are proposed as recommendations for future applications of EDFA-assisted optical systems under radiation exposure environments.

Index Terms: Optical communications, radiation effect, fiber device and optical amplifier, differential phase shift keying.

1. Introduction

High-speed, large-bandwidth and low-power-consumption free space optical communications has become a vital part of the space-ocean information networks. Superior modulation formats play an important role in expanding available bandwidth and improving long-distance transmission performances. Due to higher tolerance for noise and nonlinear effects, DPSK format has become a hot spot in modern high-speed optical communications systems [1], [2]. DPSK-based laser communication relay demonstration (LCRD) conducted by NASA [3] shows high optical communication

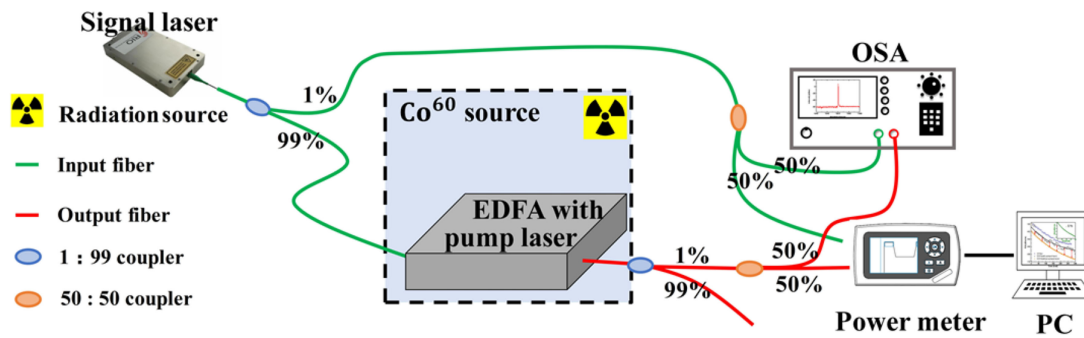


Fig. 1. Schematic diagram of the performance test system for EDFA under radiation.

data-rate. The emergence of REDFAs provides a good solution for long-distance communications, e.g., satellite communications and space applications [4]. However, RE ions always exhibit strong sensitivity to space radiation, which leads to the performance degradation of REDFAs [5], [6]. RIA is an effective measure to evaluate the susceptibility of optical fibers to irradiation environments [7]. Among numerous radiation damage effects, total ionizing dose effect and displacement damage dose effect [8] are the most important effects to form color centers. On average, for low orbit (<500 km) cases, the annual radiation dose lies between 5 krad and 50 krad, while for high-orbit (10000 ~ 20000 km) cases, the annual radiation dose can reach 250 krad. In order to elongate the orbital duration, effective anti-irradiation measures have to be taken for REDFAs.

Some radiation hardening techniques are used to suppress the above-mentioned effects, including physical shielding layer [9], photobleaching [4], thermal-bleaching [10], hole-assisted carbon coated H₂-loading [11]–[13], hollow-core photonic bandgap fibers [14] and Ce co-doping [7], [15]. Despite some earlier studies dealing with RIA of EDF, or gamma radiation effects on EDFA [16]–[18], few efforts have been put on the effects of other factors, such as *NF*, half-width and central wavelength of the output laser. In addition, the more complex *RIA-Dose* mechanism has not yet been well addressed. Moreover, since irradiation can cause permanent damages to the optical amplifier, radiation experiments are costly and very limited experimental results could be found to thoroughly analyze the radiation-induced performance degradation mechanisms. As one of the key devices in long-haul optical communications systems, so evaluating the effectiveness of anti-irradiation measures at the system level should be more meaningful.

In this work, we carried out the EDFA spectroscopy experiment under gamma radiation, and obtained the evolution law of the central wavelength, half-width, and *NF* (amplified spontaneous emission (ASE) noise) of the output laser. In order to evaluate the state-of-art anti-irradiation measures at the device level, the effects of anti-irradiation schemes are compared in a series of experiments. At the system level, we comprehensively consider the RIA, photobleaching and *NF* (ASE noise) changes of EDFA in radiation environment, and numerically investigate the influence of radiation on performances of DPSK inter-satellite laser communication based on preamplification technology (EDFA). This work is anticipated to open up new perspectives for future deep space optical communication missions.

2. Experimental Setup

Fig. 1 shows schematic diagram of the performance test system for EDFA under radiation. The EDFA is exposed to Co⁶⁰ gamma radiation at room temperature at the Institute of Isotope Research, Henan Academy of Sciences, China. It is necessary to fix all of optical fibers and ensure the stability of Co⁶⁰ source before the radiation experiment. The distance between the radiation source and EDFA is adjusted to acquire a radiation rate of 2 krad/min. The total radiation time is 150 minutes. An optical spectrum analyzer (OSA) is used in our experiment to measure the *NF* every 1 minute and

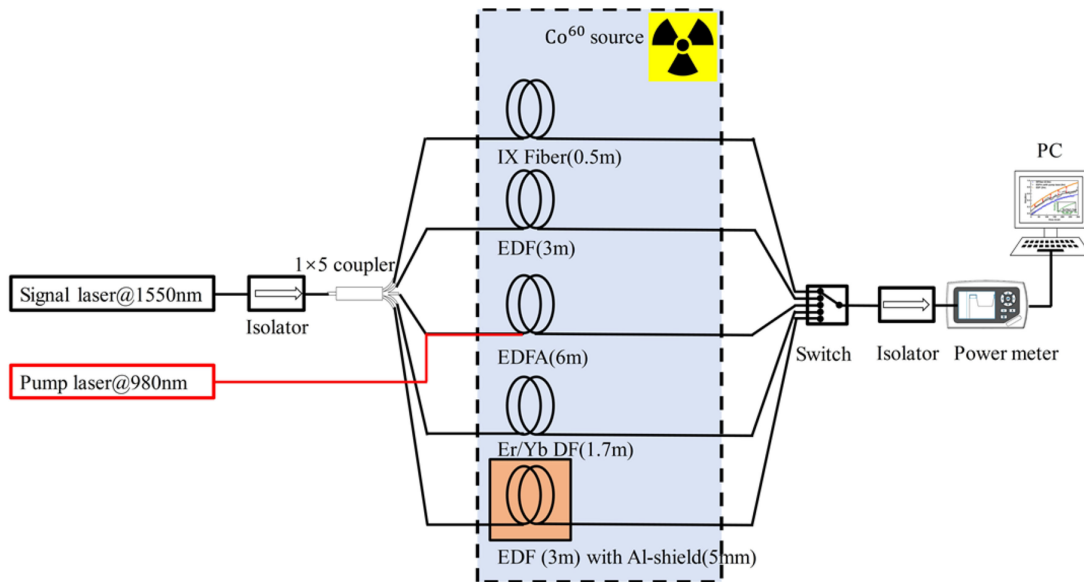


Fig. 2. Experimental setup for the tests of anti-irradiation schemes.

save the spectral data every 10 minutes. The central wavelength, linewidth and power of the signal light in our experiments are 1549.74 nm, 3 kHz and 17 mW, respectively, to meet the demand of DPSK coherent optical communication for a high-frequency stable laser with narrow linewidth laser. 1% of signal light and 1% of output light are used for spectrum monitoring and power monitoring, respectively.

Fig. 2 illustrates the experimental setup for the tests of optical fibers and EDFA. Test fibers are exposed to gamma radiation generated from a Co^{60} source at room temperature. The typical rate and the duration time of irradiation experiments are 2.09 krad/min and 191 mins, respectively, and the total dose is about 400 krad. Optical isolators are used to protect the laser from being damaged by the reflection light. Optical switch is used to select the channel. Different test fibers are used to evaluate distinct anti-irradiation methods. Power meters and computers are used to monitor real-time power fluctuation in our experiment.

As a comparison experiment, 16.8 mW signal light is launched into the EDF (The only difference between EDF and EDFA is that there is no pump laser). All fibers employed in our experiments are produced from the same batch of optical fibers manufactured by OFS [19] to ensure the same experimental condition, conventional optical fibers produced by IXblue [20] having six holes filled with H_2 in silica cladding and Ce ions in the fiber core are employed (Fig. 3) in H_2 -loading and Ce co-doping schemes. Based on finite element method, we have simulated the mode field distribution and normalized electric field intensity distribution of this unique fiber at 1550 nm and 980 nm, respectively. As shown in Fig. 3, the cladding holes do not affect the transmission of the guided core mode. In order to induce photobleaching effect, EDFA with 980 nm pump power of 398 mW is applied. For the shielding layer method, a 5 mm thick aluminum (Al) plate is used to package the EDF. In order to study the effect of co-doping other RE ions, Er/Yb co-doping is investigated. Since radiation will cause permanent damages, all optical fibers can be used for single radiation test.

3. Experimental Results and Discussion

Fig. 4(a) shows spectral evolution under different radiation doses. It could be seen that central wavelength of the output laser is stable at 1549.74 nm even at high dose levels (>250 krad), which is consistent with the experimental results reported in [21]. However, data fitting indicates that

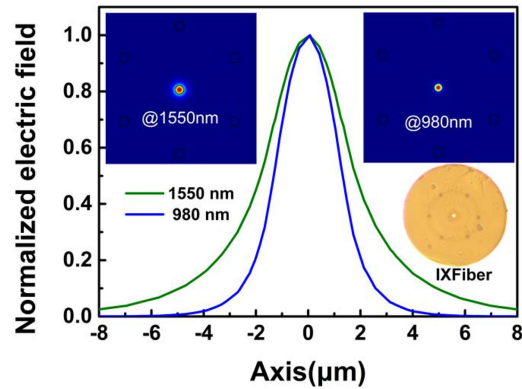


Fig. 3. Normalized electric fields at 1550 nm and 980 nm, respectively. Inset gives the IXFiber structure and the guided mode distribution.

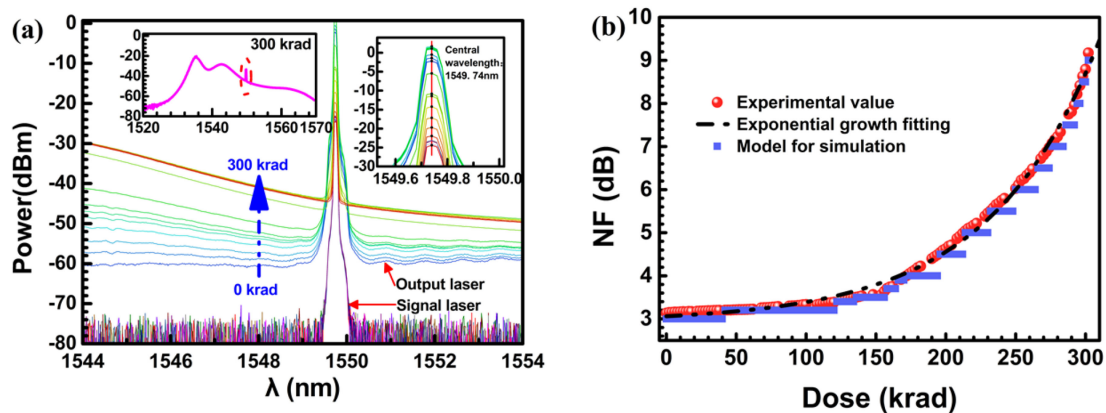


Fig. 4. (a) Spectral evolution and (b) NF of EDFA as a function of radiation dose.

the FWHM becomes narrower with the increment of radiation dose (The variation ratio is about 1.69×10^{-4} nm/krad). The maximum gain of the EDFA is approximately 25 dB. The output power decreases in a fluctuation way as radiation dose increases, which is due to temperature effect on electro-optic efficiency of the pump laser. The output spectrum within 1520–1570 nm at 300 krad is given in this figure. It can be seen that the amplified signal light has submerged in the ASE noises. The strong spontaneous emission effect indicates that the amplifier operates in a small signal model, and the radiation suppresses the interaction of Er^{3+} ions on the metastable state with photons. The noise floor of the output spectrum increases with the increment of radiation dose, particularly in the short-wave side of the central wavelength due to the ASE peak position. The *NF* is given by the OSA through spectral comparison of the input and output light, as shown in Fig. 4(b). *NF* growth turns out exponential increase trend as radiation dose increases. Maximum *NF* reaches ~9 dB when radiation dose is 300 krad. Unlike the fluctuating behavior of output power, *NF* exhibits a steady increase, which reflects the radiation effect on spontaneous emission. Therefore, in future work, we would focus on the method to suppress the radiation-induced ASE noises.

As shown in Fig. 5, as the irradiation dose increases, different radiation hardened methods show an increase in RIA, which reflects a certain degree of degradation of output performances. For general EDF, when the radiation dose reaches 300 krad, the RIA value reaches about 0.94 dB/m. The physical shielding layer scheme shows that the Al box (5 mm thick) plays a role in protecting the fiber under lower dose radiation. However, as the radiation dose increases, the protection effect is getting worse and worse. When it reaches ~250 krad, its RIA value is the same as that of a general

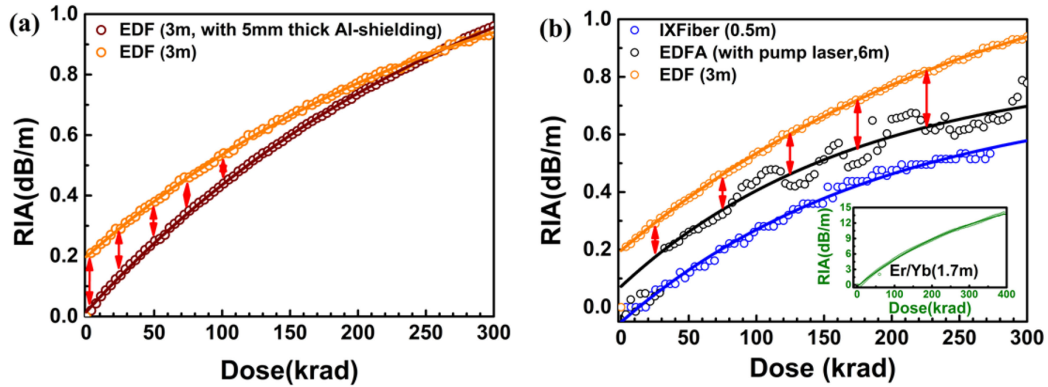


Fig. 5. Test results of RIA in different anti-irradiation schemes (a) Al shielding layer (b) IXFiber (H_2 loading and Ce co-doping), photobleaching and Er/Yb co-doped fiber.

EDF. The protection range of radiation dose is limited due to the thickness of the shielding layer, which can be explained by Beer-Lambert law ($T = e^{-\mu d}$ where T is the radiation transmittance, μ is the attenuation coefficient, and d is the sample thickness). We can see the obvious improvement in anti-irradiation effect (restored $\sim 25.4\%$ at 300 krad) when the pump light is added to induce photobleaching. The solid line fit in Fig. 5 is based on the RIA power law [22], which is a semi-empirical formula related to radiation dose. Within a certain range, as the radiation dose increases, the photobleaching gain effect becomes stronger (the arrows in the Fig. 5(b)). This is due to the increasing number of repairable injuries that ionizing radiation produces. It can be predicted that when the radiation dose is large enough, the irreparable radiation damage will also increase, and the photobleaching effect will be suppressed. IXFiber shows best radiation resistance performances (restored $\sim 46.5\%$ at 300 krad) under the above conditions. This is due to the comprehensive outcome of the presence of Ce^{3+} (Ce^{4+}) and the suppression of the absorption band caused by the radiation-generated electrons (holes) [23]. Moreover, the Si-H bonding and the O-H bonding will absorb the radiant energy in part [24], [25]. Er/Yb co-doped fiber experimental results show the greatest sensitivity to irradiation (~ 14 dB/m at 300 krad), which may be related to the color center formed around Yb ions. The experimental results give the ordering of the above anti-irradiation measures and prove the importance of optimizing the doped fiber structure [15] in anti-irradiation schemes.

4. System Simulation Model

The anti-irradiation schemes described above is intended for applications in space missions. In this section, we will study the effects of EDFA performance degradation in DPSK systems under gamma radiation. Since there is no repeater between the transmitter and the receiver in space laser communication, the EDFA (or other amplifier) has to be used as the pre-amplifier at the receiving end [26]. In our model, main effects of radiation on EDFA through experimental results include two aspects: gain attenuation (RIA) and ASE noise (NF). The link distance is 1000 km and the communication data rate is 40 Gbps. Channel attenuation, ASE noise of EDFA, photodetector noise and its responsivity are considered in this model. Optical transmitter based on differential encoding is shown in Fig. 6(a). Our transmit part uses a binary sequence to perform differential pre-coding, and then a non-return-to-zero (NRZ) pulse is generated by the NRZ pulse generator into a Mach-Zehnder modulator. The optical carrier generated by the laser is connected with the other end of the one-stage Mach-Zehnder modulator. In this consideration, the information sequence pulse could be described as:

$$s(t) = \sum_{n=-\infty}^{\infty} a_n g(t - nT_b) \quad (1)$$

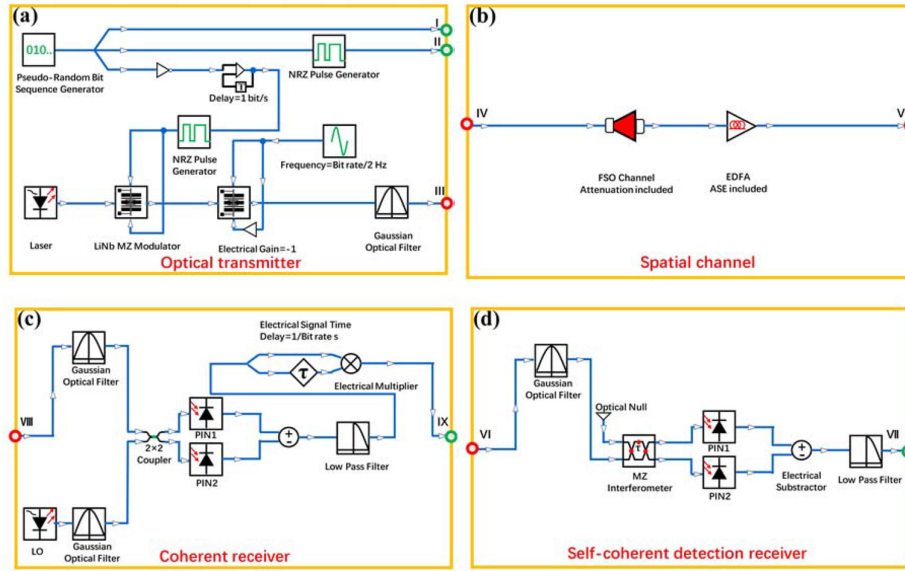


Fig. 6. (a) Schematic diagram of DPSK optical transmitter. (b) Space channel. (c) The DPSK homodyne coherent detection receiver. (d) The self-coherent detection receiver.

where a_n represents information on the n th bit, which is 0 or 1, $g(t)$ represents a rectangular pulse function, and T_b is a bit period. The bias voltage (peak to peak value is $2V_\pi$) is set at the lowest point on the Mach-Zehnder modulator bias curve, and the input drive voltage can be written as:

$$V_{in1} = 2V_\pi \sum_{n=-\infty}^{\infty} a_n g(t - nT_b) - 2V_\pi \quad (2)$$

Therefore, the output light field and optical power are:

$$E_{out1} = E_{in1} \cos\left(\frac{\pi}{2V_\pi} V_{in1}\right) e^{j\pi/2} = \pm j E_{in1}(t) \quad (3)$$

$$P_{out1} = P_{in1} \cos\left(\frac{\pi}{2V_\pi} V_{in1}\right) e^{j\pi/2} = P_{in1}(t) \quad (4)$$

It can be seen that the phase of the output light field is voltage dependent while the output power is constant.

Then the sine wave generator with a frequency of half the transmission rate controls the second-stage Mach-Zehnder modulator and simultaneously segment the previously generated NRZ signal to obtain the RZ signal carrying the phase information.

The input drive voltage applied on the second-stage Mach-Zehnder modulator can be written as:

$$V_{in2} = V_\pi \sin(\omega_0 t/2) \quad (5)$$

Finally, the optical field and optical power of the output RZ-DPSK modulation are:

$$E_{out2} = E_{out1} \cos(V_{in2}) = \pm j E_{in1} \cos\left(V_\pi \sin\left(\frac{\omega_0 t}{2}\right)\right) \quad (6)$$

$$P_{out2} = P_{out1} \cos(V_{in2}) = \pm j P_{in1} \cos\left(V_\pi \sin\left(\frac{\omega_0 t}{2}\right)\right) \quad (7)$$

Free space optical transmission attenuation, geometric loss of transmitter and receiver are all considered in the channel model.

$$P_{\text{Rec}} = P_{\text{Tra}} \frac{d_R^2}{(d_T + \theta R)^2} 10^{-\alpha R/10} \quad (8)$$

where P_{Rec} , P_{Tra} , d_R , d_T , θ , α and R refer to received power, transmit power, receiver aperture, transmitter aperture, beam angle, spatial attenuation and link distance, respectively.

ASE noise is considered in the EDFA based on gain control model in Fig. 6(b).

The EDFA gain can be expressed as:

$$G = \frac{(P_{\text{out}} - P_{\text{ASE}})}{P_{\text{in}}} \quad (9)$$

where G , P_{out} , P_{in} and P_{ASE} are gain, output power, input power and ASE power, respectively.

Considering the presence of ASE in the input signal, the output ASE spectral density $S_{\text{out}}(\lambda)$ can be expressed as:

$$S_{\text{out}}(\lambda) = S_{\text{amp}}(\lambda) + S_{\text{in}}(\lambda) \times G \quad (10)$$

where $S_{\text{amp}}(\lambda)$ and $S_{\text{in}}(\lambda)$ are ASE spectral density of EDFA and input signal, respectively.

Therefore, NF can be written as:

$$NF \text{ (dB)} = 10 \lg \left[\frac{1}{G} + \frac{S_{\text{out}}|_{\lambda=\lambda_s}}{G h \nu} - \frac{S_{\text{in}}|_{\lambda=\lambda_s}}{h \nu} \right] \quad (11)$$

where $1/G$, λ_s , h and ν are shot noise, signal wavelength, planck constant and signal frequency, respectively.

We use NF to evaluate the output ASE:

$$S_{\text{out}}|_{\lambda=\lambda_s} = \left[G h \nu [10^{NF/10} - \frac{1}{G} + \frac{S_{\text{in}}|_{\lambda=\lambda_s}}{h \nu}] \right] \quad (12)$$

The ASE spectrum can be obtained using the input parameters of NF and G .

As shown in Fig. 6, two DPSK demodulation schemes are considered. One is based on homodyne coherent detection, as shown in Fig. 6(a), Fig. 6(b) and Fig. 6(c), respectively, while the other is based on self-coherent detection, as illustrated in Fig. 6(a), Fig. 6(b) and Fig. 6(d), respectively. The red circles of each module in Fig. 6 represent the connection points between different modules, and the green circles are the nodes used for BER test. In the homodyned coherent system, the operation wavelengths of the local oscillator (LO) and the signal light are both fixed at 1550 nm, and the output power is about 1 mW. After signal mixing, the absolute code is restored using differential coherent interrogation methods. In self-coherent detection system, phase information carried in DPSK is transformed into amplitude information by a time-delay Mach-Zehnder interferometer, while the optical signal is transferred to two PIN photodiodes through the balanced detection circuit to ultimately acquire the signal details.

5. Simulation Results and Discussion

We have simulated the communication quality of different EDFA anti-irradiation schemes, as shown in Fig. 7(a). Some factors were considered in the numerical model of the amplifier. In the presence of pump laser, the EDFA performance would improve due to the ‘‘photobleaching’’ phenomenon. In the first step, we need to figure out the RIA -Dose of EDFA (RE doped fibers with pump laser) for the IXFiber structure and AI shielding layer schemes, respectively. Assuming that the fiber doping concentration and the pump power are the same for the above two schemes, and according to the measurement results of RIA -Dose experiments for EDF(g_{EDF}) and EDFA(g_{EDFA}), a transfer function could be described as:

$$f = g_{\text{EDFA}}/g_{\text{EDF}} \quad (13)$$

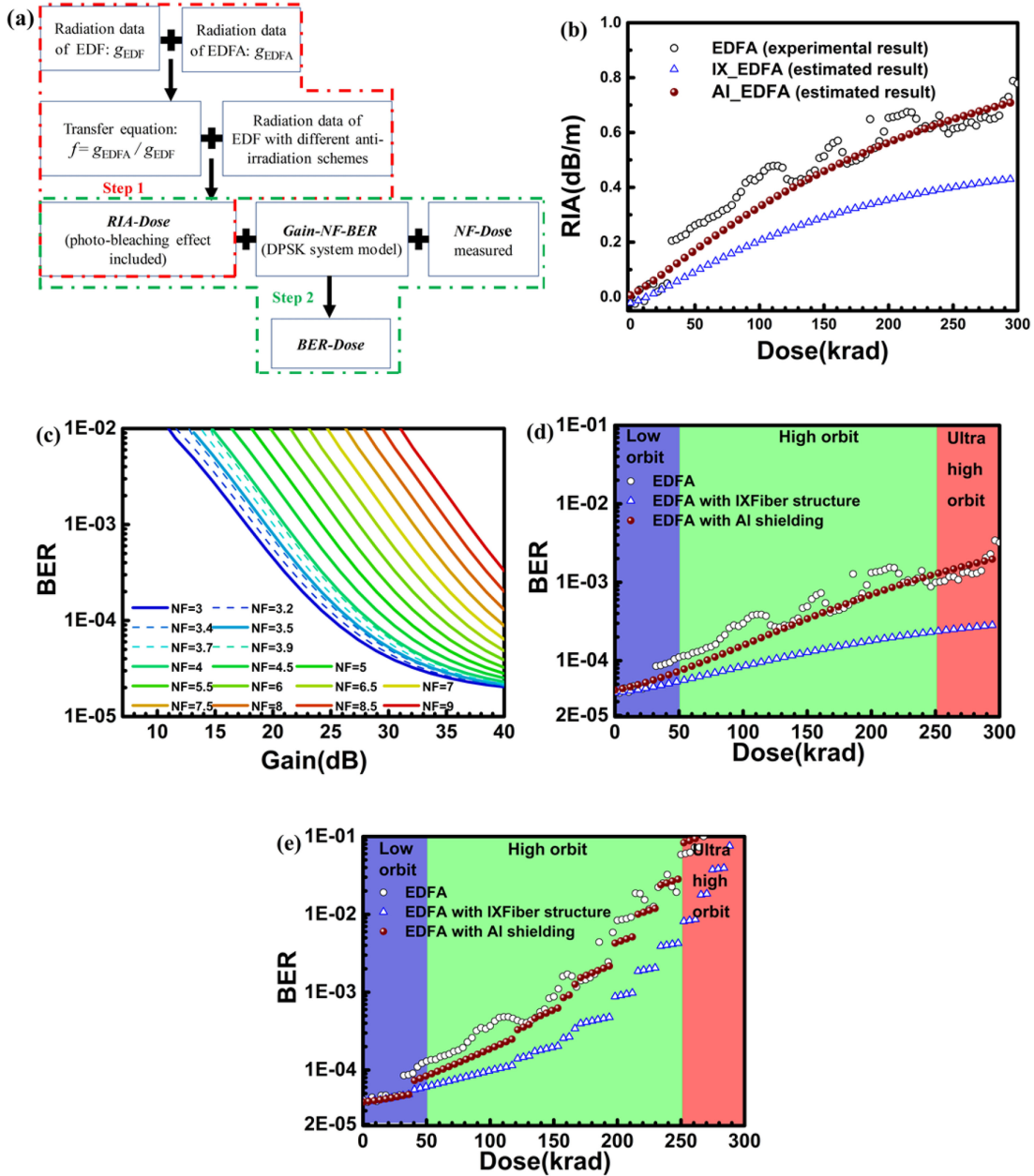


Fig. 7. (a) Simulation flowchart. (b) Estimated $RIA-Dose$ of EDFA for different anti-irradiation schemes. (c) $Gain-NF-BER$ curve of DPSK coherent communication systems. (d) Radiation effect on the system BER for different anti-irradiation schemes (including RIA only, $NF = 3.4$ dB). (e) Radiation effect on the system BER for different anti-irradiation schemes. (including RIA and the radiation effect on NF).

By using the experimental results in the two schemes ($g_{IX,EDF}$ and $g_{AI,EDF}$) and the transfer function f , the estimated $RIA-Dose$ ($g_{IX,EDFA}$ and $g_{AI,EDFA}$) of the EDFA applied in the two schemes could be expressed by the following equations (Fig. 7(b)):

$$g_{IX,EDFA} = g_{IX,EDF} \times f, \quad (14)$$

$$g_{AI,EDFA} = g_{AI,EDF} \times f. \quad (15)$$

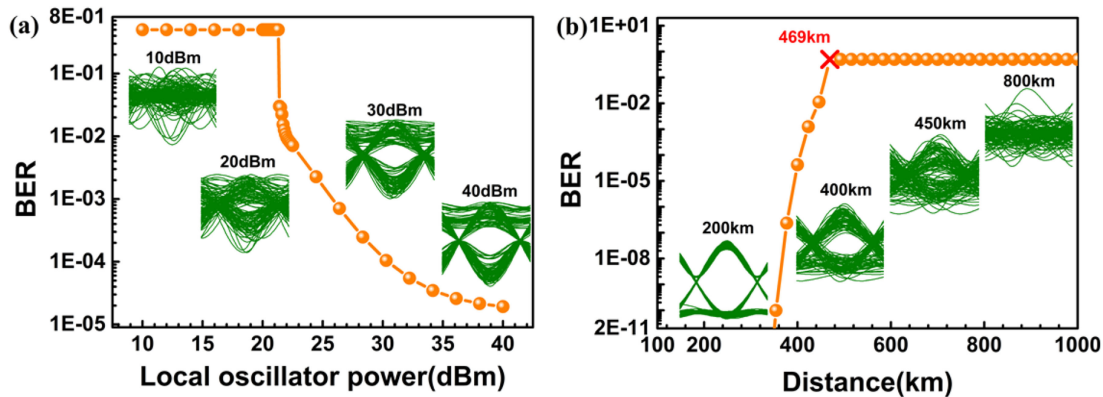


Fig. 8. (a) LO power impact on BER of coherent systems. (b) Relationship between link distance and BER for self-coherent systems.

In the second step, taking the homodyne coherent detection system as an example, the *Gain-NF-BER* feature of DPSK communication system can be calculated (Fig. 7(c)). Based on the experimentally measured *NF-Dose* relationship of the EDFA, we use a segmentation model (Fig. 4(b)) to describe the experimental results for combination with discrete *Gain-NF-BER* curve in the simulation. Further, when REDF length is 20 m and initial gain is 25 dB, in combination with the *RIA-Dose* relationship acquired in step one, the influence of different schemes on BER could be obtained, as shown in Fig. 7(e).

From Fig. 7(c), the system BER decreases as gain increases while increases with the increment of *NF* (ASE noise). It can be seen that *NF* is a key factor that determines the flatness of the *Gain-BER* curve. In the case that the radiation effect on *NF* is negligible, Fig. 7(d) gives the simulation result when *NF* is set to 3.4 dB. At the system level, the physical shielding layer would only work for low-orbit cases. When the dose reaches 300 krad, compared to their initial level, the system BER of EDFA without anti-radiation protection and EDFA with IXFiber structure increases by ~ 18.88 dB and ~ 8.69 dB, respectively. Fig. 7(e) shows the radiation effect on *NF* and RIA. It is clear that the irradiation effect on the system BER would increase with the increment of radiation dose. When the dose reaches 300 krad, the system BER of the EDFA without anti-radiation protection and the EDFA with IXFiber structure would increase by ~ 43.83 dB and ~ 37.28 dB, respectively. The above analysis shows that for pre-amplification-based communication systems, compared to RIA effect, the impact of radiation on *NF* would play a more important role in degrading the communications quality. Since the strong absorption of the color center leads to an increase in *NF*, some measures to suppress the color center are required. For example, to increase the pump laser power to induce the photobleaching effect or to provide a high and low temperature cycle environment to induce thermal annealing effect and so on.

In addition to the anti-irradiation measures as described above, what should we do at the system level for radiation-induced attenuation? In homodyne coherent detection system, the signal photocurrent generated by the photodetector can be expressed as: $I_s(t) = 2R\sqrt{P_s(t)P_L}$, where R denotes responsiveness of the detector, P_s , P_L are signal power and LO power, respectively. It can be seen that the LO acts as an amplifier in the coherent detection scheme, and the receiving sensitivity of the signal is also improved. In the simulation, the link loss is first introduced to interrupt the communication. Then, by increasing the LO power, it can be seen that the system performances gradually increase, and the eye diagram becomes increasingly clear, as shown in Fig. 8(a). Therefore, improving the LO power and matching a reasonable filter is a solution to overcome the radiation attenuation, but its power increase still depends on the fiber amplifier. That is to say, we should leave enough margin for signal amplification.

In the self-coherent detection system (Fig. 8(b)), the link distance cannot reach 1000 km under the same channel condition, and the critical distance of communication recovery is 469 km (less

than half of the communication distance of the coherent detection system), this is due to the fact that the DPSK self-coherent detection system is ultimately based on amplitude detection. However, homodyne coherent detection system requires high-purity spectral sources and high mixing efficiency, etc, which increases the system complexity. For short-range satellite communications, the self-coherent detection system demonstrates excellent communication quality.

6. Conclusion

The exponential growth of NF in response to the radiation dose makes it necessary to include the impact of NF (ASE noise) in the simulation model besides RIA effects. The RIA of fibers and amplifiers for different anti-irradiation schemes has been experimentally tested by Co^{60} source. Total radiation dose is gradually increased to 300 krad to simulate device performance degradation for different orbital cases. These results show that the anti-irradiation performance from high to low are IXFiber (H_2 -loading technology and Ce ion doping), photobleaching and Al shielding layer. In system simulation, our model considers the photobleaching effect, RIA effect, and experimentally measured ASE noise. It can be clear that the the physical shielding layer would no longer work well for the middle- and high-orbit cases due to its limited thickness. In the past, numerous studies have been concentrated on the RIA effect. Through system simulation, we find that the radiation-induced increase in NF would bring about more deadly damages to the communications system than RIA effect alone. In addition, LO power boost helps to improve system performances when RIA occurs; homodyne coherent detection system has higher detection sensitivity, while self-coherent detection system has simpler structure and is suitable for systems with high signal to noise ratio.

Acknowledgment

We would like to thank the anonymous reviewers for their constructive suggestions and also express our gratitude to X. Zhang for her help on English revision.

References

- [1] X. Huang *et al.*, "Performance comparison of all-optical amplify-and-forward relaying FSO communication systems with OOK and DPSK modulations," *IEEE Photon. J.*, vol. 10, no. 4, Aug. 2018, Art. no. 7905411.
- [2] Y. Su *et al.*, "10 Gbps DPSK transmission over free-space link in the mid-infrared," *Opt. Exp.*, vol. 26, no. 26, 2018, Art. no. 34515.
- [3] B. L. Edwards *et al.*, "Overview of the laser communications relay demonstration project", in *Proc. SpaceOps*, 2012, Art. no. 1261897.
- [4] A. Ladaci *et al.*, "Optimized radiation-hardened erbium doped fiber amplifiers for long space missions," *J. Appl. Phys.*, vol. 121, no. 16, 2017, Art. no. 163104.
- [5] Y. Kobayashi, E. H. Sekiya, K. Saito, R. Nishimura, K. Ichii, and T. Araki, "Effects of Ge Co-doping on P-related radiation-induced absorption in Er/Yb-doped optical fibers for space applications," *J. Lightw. Technol.*, vol. 36, no. 13, pp. 2723–2729, Jul. 2018.
- [6] S. Girard *et al.*, "Radiation effects on ytterbium- and ytterbium/erbium-doped double-clad optical fibers," *IEEE Trans. Nucl. Sci.*, vol. 56, no. 6, pp. 3293–3299, Dec. 2009.
- [7] A. Ladaci *et al.*, "Radiation hardened high-power Er(3+)/Yb(3+)-codoped fiber amplifiers for free-space optical communications," *Opt. Lett.*, vol. 43, no. 13, pp. 3049–3052, Jul. 2018.
- [8] X. Hou *et al.*, "Review of radiation hardening techniques for EDFAs in space environment," *Proc. SPIE*, vol. 9521, 2015, Art. no. 95211D1.
- [9] F. A. Cucinotta, "Review of NASA approach to space radiation risk assessments for Mars exploration," *Health Phys.*, vol. 108, no. 2, pp. 131–142, Feb. 2015.
- [10] S. Girard *et al.*, "Radiation effects on silica-based optical fibers: recent advances and future challenges," *IEEE Trans. Nucl. Sci.*, vol. 60, no. 3, pp. 2015–2036, Jun. 2013.
- [11] S. Girard *et al.*, "Radiation-hard erbium optical fiber and fiber amplifier for both low- and high-dose space missions," *Opt. Lett.*, vol. 39, no. 9, pp. 2541–2544, May 2014.
- [12] S. Girard *et al.*, "On-site regeneration technique for hole-assisted optical fibers used in nuclear facilities," *IEEE Trans. Nucl. Sci.*, vol. 62, no. 6, pp. 2941–2947, Dec. 2015.
- [13] S. Girard *et al.*, "Proton irradiation response of hole-assisted carbon coated erbium-doped fiber amplifiers," *IEEE Trans. Nucl. Sci.*, vol. 61, no. 6, pp. 3309–3314, Dec. 2014.
- [14] S. Girard, J. Baggio, and J. L. Leray, "Radiation-induced effects in a new class of optical waveguides: The air-guiding photonic crystal fibers," *IEEE Trans. Nucl. Sci.*, vol. 52, no. 6, pp. 2683–2688, Dec. 2005.

- [15] S. Girard *et al.*, "Radiation hardening techniques for Er/Yb doped optical fibers and amplifiers for space application," *Opt. Exp.*, vol. 20, no. 8, pp. 8457–8465, Apr. 2012.
- [16] D. M. Boroson *et al.*, "Radiation influence on Er/Yb doped fiber amplifiers performances: high power and WDM architectures," *Proc. SPIE*, vol. 10524, 2018, Art. no. 10524101.
- [17] E. Haddad *et al.*, "Comparison of gamma radiation effect on erbium doped fiber amplifiers," *Proc. SPIE*, vol. 10562, 2017, Art. no. 10562191.
- [18] D. Gunn, G. C. Valley, and T. S. Rose, "Gamma and proton radiation effects in erbium-doped fiber amplifiers: Active and passive measurements," *J. Lightw. Technol.*, vol. 19, no. 12, pp. 1918–1923, Dec. 2001.
- [19] OFS Company, 2016. [Online]. Available:<http://fiber-optic-catalog.ofsoptics.com/category/erbium-doped-optical-fiber>
- [20] IXBlue Photonics, 2015. [Online]. Available:<https://photonics.ixblue.com>
- [21] M. Li *et al.*, "Investigation of the irradiation effect on erbium-doped fiber amplifiers composed by different density erbium-doped fibers," *Laser Phys.*, vol. 19, no. 1, pp. 138–142, 2009.
- [22] M. Lezius *et al.*, "Radiation induced absorption in rare earth doped optical fibers," *IEEE Trans. Nucl. Sci.*, vol. 59, no. 2, pp. 425–433, Apr. 2012.
- [23] J. S. Stroud, "Color centers in a cerium-containing silicate glass," *J. Chem. Phys.*, vol. 37, no. 4, pp. 836–841, 1962.
- [24] F. Messina and M. Cannas, "In situ observation of the generation and annealing kinetics of E' centres induced in amorphous SiO(2) by 4.7 eV laser irradiation," *J. Phys. Condens Matter*, vol. 17, no. 25, pp. 3837–3842, Jun. 2005.
- [25] K. Kajihara, L. Skuja, M. Hirano, and H. Hosono, "In situ observation of the formation, diffusion, and reactions of hydrogenous species in F2-laser-irradiated SiO2 glass using a pump-and-probe technique," *Phys. Rev. B*, vol. 74, no. 9, 2006, Art. no. 094202.
- [26] J. Ma, M. Li, L. Tan, Y. Zhou, S. Yu, and Q. Ran, "Experimental investigation of radiation effect on erbium-ytterbium co-doped fiber amplifier for space optical communication in low-dose radiation environment," *Opt. Exp.*, vol. 17, no. 18, pp. 15571–15577, Aug. 2009.